RSC Advances

PAPER

View Article Online
View Journal | View Issue

Cite this: *RSC Adv.*, 2016, **6**, 20120

TiO_2–multi-walled carbon nanotube nanocomposites: hydrothermal synthesis and temporally-dependent optical properties†

Aijian Wang,[abc] Yun Wang,[a] Wang Yu,[a] Zhipeng Huang,[a] Yu Fang,[d] Lingliang Long,[a] Yinglin Song,[d] Marie P. Cifuentes,[e] Mark G. Humphrey,[e] Long Zhang,[c] Jianda Shao[c] and Chi Zhang*[bce]

Received 14th December 2015
Accepted 27th January 2016

DOI: 10.1039/c5ra26677g

www.rsc.org/advances

Multi-walled carbon nanotube (MWCNT)/TiO_2 nanocomposites have been prepared by a hydrothermal method and characterized by Fourier-transform infrared, Raman, and X-ray photoelectron spectroscopies, X-ray powder diffraction, and transmission electron microscopy. Their viability as nonlinear optical (NLO) materials has been examined using the Z-scan technique at 532 nm with both nanosecond and picosecond laser pulses, the NLO and optical limiting (OL) performance being found to be dependent on the TiO_2 content. At the wavelength used, an enhanced OL response was observed for the M1.00 nanocomposite and ascribed to a combination of mechanisms.

Introduction

Because multi-walled carbon nanotubes (MWCNTs) are usually assembled from a large number of concentric graphitic tubes,[1] they are preferable to single-walled carbon nanotubes (SWCNTs) as components of electron donor–acceptor ensembles.[2,3] MWCNTs have been the subject of intense scrutiny due to their unique mechanical, electronic and optical properties.[4] MWCNTs have attracted particular attention in chemistry, with many reports of MWCNT nanocomposites that tune the MWCNTs' properties and, in particular, a number suggesting that they are good candidates for the fabrication of optoelectronic devices.[5–12] For example, phthalocyanine- and porphyrin-covalently-functionalized MWCNT nanocomposites exhibit strong OL responses due to reverse saturable absorption (RSA) and nonlinear scattering.[13,14] However, although phthalocyanine and porphyrin usually exhibit a strong OL performance, a lack of thermal stability and optical bleaching limit their potential applications.

MWCNT-based materials that include semiconductors may be expected to overcome this drawback, due to the long-term chemical inertness of the latter against photocorrosion.[15] TiO_2, with a wide bandgap of *ca.* 3.2 eV, has received considerable attention both in optoelectronic and protective applications because of its high transparency in the visible region, excellent mechanical durability, photostability, chemical stability, and unique electronic and optical properties.[16] TiO_2 and MWCNTs possess excellent properties in isolation, and their nanocomposites may possess enhanced or novel behavior compared to those of the individual units. TiO_2 has been used previously to prepare MWCNT/TiO_2 nanohybrids for photocatalytic and solar cell applications,[17,18] but the use of such nanohybrids to fabricate optoelectronic devices with superior OL performance has not been reported, although the nonlinear optical properties of a range of nanoscale composite materials containing TiO_2 have been explored.[19–24]

Previous studies of MWCNT/TiO_2 materials have highlighted the interesting properties of nanocomposites obtained by a variety of approaches.[21,25] Herein, and inspired by the findings above, we have explored combining TiO_2 nanoparticles with MWCNTs by a simple hydrothermal treatment of tetrabutyl titanate and MWCNTs in EtOH–H_2O mixtures. The composition and structure of these TiO_2/MWCNT nanocomposites have been elucidated by Fourier-transform infrared, Raman, and X-ray photoelectron spectroscopies, X-ray powder diffraction, and transmission electron microscopy. The influence of TiO_2 content on the NLO behavior of the TiO_2/MWCNT nanocomposites has been systematically investigated by evaluating the effect of different ratios of MWCNT : TiO_2.

[a]*China-Australia Joint Research Center for Functional Molecular Materials, Scientific Research Academy, Jiangsu University, Zhenjiang 212013, P. R. China*

[b]*China-Australia Joint Research Center for Functional Molecular Materials, School of Chemical and Material Engineering, Jiangnan University, Wuxi 214122, P. R. China. E-mail: chizhang@jiangnan.edu.cn; Fax: +86-510-85917763*

[c]*Key Laboratory of Materials for High-Power Laser, Shanghai Institute of Optics and Fine Mechanics, Chinese Academy of Sciences, Shanghai 201800, P. R. China. E-mail: czhang@siom.ac.cn*

[d]*School of Physical Science and Technology, Soochow University, Suzhou 215006, P. R. China*

[e]*Research School of Chemistry, Australian National University, Canberra, ACT 2601, Australia. E-mail: chi.zhang@anu.edu.au*

† Electronic supplementary information (ESI) available. See DOI: 10.1039/c5ra26677g

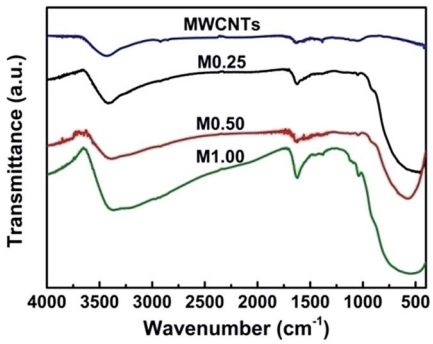

Fig. 1 FTIR spectra of MWCNTs, M0.25, M0.50 and M1.00.

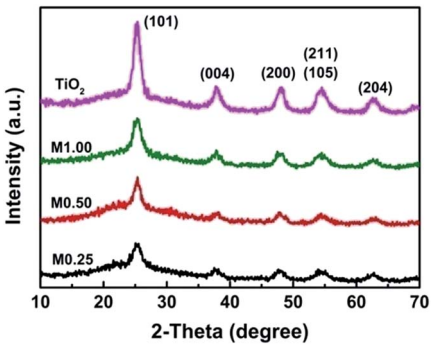

Fig. 2 XRD patterns of the TiO_2, M0.25, M0.50 and M1.00 samples.

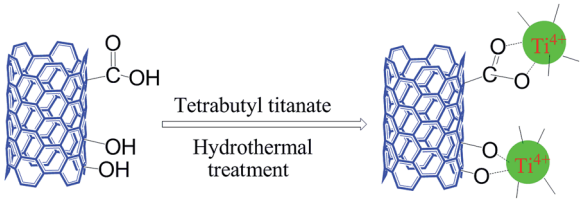

Scheme 1 Suggested attachment of TiO_2 nanoparticles to MWCNTs.

Results and discussion

Characterization

Fig. 1 displays the FTIR spectra of the pristine MWCNTs and the TiO_2/MWCNT nanocomposites (M0.25, M0.50 and M1.00). The presence of –OH groups and water on the surface of the samples was confirmed by the appearance of a broad band at *ca.* 3400 cm^{-1}, with another band at 1625 cm^{-1} corresponding to the Ti–O–H bending vibration.[26] The IR spectra reveal that the functional groups on the nanocomposites are primarily the surface groups on TiO_2; no characteristic IR bands from MWCNTs were observed in the region 400–2000 cm^{-1} because of the low percentage of MWCNTs in the composites. A peak due to stretching and binding modes of Ti–O and O–Ti–O is clearly seen near 500 cm^{-1}, while the peak at 500 cm^{-1} in the spectrum of M0.25, which is sharper than those of the other composites, may be assigned to the changing size and crystallinity.[26] The characteristic peak of TiO_2 is very broad, obscuring the fingerprint regions in the three nanocomposites, and thereby rendering them difficult to assign uniquely. The peak at 1039 cm^{-1} results from Ti–O–C vibrations, which indicates that TiO_2 has reacted with the –OH or –COOH groups (the presence of the oxygen-containing functional groups can be confirmed from the XPS spectrum of the MWCNTs in Fig. S1†) at the MWCNTs' surface by a dehydration reaction (Scheme 1).[18]

The crystalline phases of pure TiO_2 and the TiO_2/MWCNT nanocomposites (M0.25, M0.50 and M1.00) have been investigated by XRD, the results being shown in Fig. 2. It is clear that pristine TiO_2 and the TiO_2/MWCNT nanocomposites with different weight addition ratios of TiO_2 exhibit similar XRD patterns. The peaks match those of the XRD pattern of anatase TiO_2, with no observable diffraction peaks at 27° or 31°, suggesting that the TiO_2 deposited on the MWCNTs is free of rutile and brookite impurities.[27,28] The average sizes of the TiO_2 nanoparticles on the surface of the MWCNTs, which were calculated by using the Debye–Scherrer equation based on the full width at half-maximum of the diffraction peaks, are 18.9,

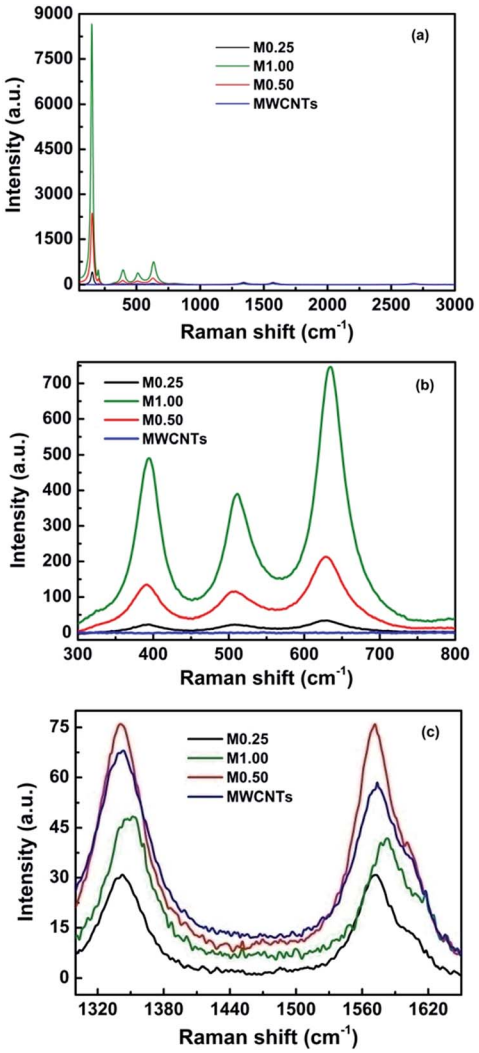

Fig. 3 (a) Raman spectra of the MWCNTs, M0.25, M0.50 and M1.00 samples; (b) expansion of the region between 300 and 800 cm^{-1}; (c) expansion of the region between 1300 and 1650 cm^{-1}.

15.4 and 13.1 nm for M0.25, M0.50 and M1.00, respectively. This result is consistent with the increase in the mass ratio of tetrabutyl titanate (the precursor of TiO_2)/MWCNTs from 5 : 1 to 10 : 1 and 20 : 1. A tiny but definitive shift is observed for the XRD peak positions, implying substantial changes in the lattice parameters.[29] The lattice parameters *a* of the anatase phase in M0.25, M0.50 and M1.00 were determined to be 3.8089, 3.8021 and 3.7916 Å, with the lattice parameters *c* ranging from 9.9815 to 10.2791 and 9.5244 Å, respectively. This also indicates that the hydrothermal process results in real integration at the interface rather than the formation of a mixture. This is confirmed *via* Raman analysis.

Raman spectra can distinguish between rutile and anatase phases and the MWCNTs. Rutile and anatase TiO_2 consist of four ($B_{1g} + E_g + A_{1g} + B_{2g}$) and six ($A_{1g} + 2B_{1g} + 3E_g$) Raman active modes, respectively. In this experiment, five characteristic bands were observed at *ca.* 152, 197, 399, 513, and 636 cm^{-1} for the TiO_2/MWCNT composites (Fig. 3a and b), corresponding to the E_g, E_g, B_{1g}, $A_{1g} + B_{1g}$, and E_g modes of anatase, respectively. The peak intensity of the E_g mode increases and the width broadens with increasing TiO_2 content. We note that both particle size and the presence of defects can influence the Raman spectra;[30] the latter is likely to be the source of the Raman band broadening in the present case.[30] The other two peaks observed at 1344 and 1574 cm^{-1} are, respectively, attributed to the characteristic D and G bands of MWCNTs, corresponding to the disordered A_{1g} mode and the tangential E_{2g} mode (Fig. 3c).[31] The disordered A_{1g} mode suggests imperfection of the sp^2 hybridization of the MWCNTs, which may originate from the production process or the surface modification process. The relative intensity ratio of D to G band (I_D/I_G) is sensitive to the surface character of the MWCNTs, and is an indication of disorder in the MWCNTs. In our case, the I_D/I_G ratio is 1.14 for the MWCNTs, decreasing to 0.99 and 1.00 for M0.25 and M0.50, respectively. However, the I_D/I_G rises slightly to 1.16 for M1.00, which suggests increased defects on the MWCNTs.[31] The Raman spectra together with the XRD patterns provide sufficient evidence to verify the incorporation of TiO_2 in the composites. The ratio of the TiO_2 incorporated at the MWCNTs' surfaces can be estimated by the integrated intensity ratio of the E_g anatase peak (I_A) and the disordered carbon peak (I_D) of the Raman spectra. As shown in Table 1, the I_A/I_D intensity of M1.00 is greater than those of M0.25 and M0.50, indicating that there is more TiO_2 deposited on the MWCNTs surface in M1.00 than in M0.25 and M0.50.[32]

The loading of the TiO_2 nanoparticles onto the MWCNTs' surfaces was characterized by TEM, typical images of the MWCNTs and the TiO_2/MWCNT nanocomposites being shown in Fig. 4. The morphology of the pristine MWCNTs is quite typical, with chaotic orientation of readily-distinguishable single nanotubes. There is a relatively smooth and clean surface without any extra phase on the surface (Fig. 4a), and the hollow structure of the MWCNTs can be clearly seen. TEM micrograph comparisons of MWCNTs (Fig. 4a) and the TiO_2/MWCNT nanocomposites (Fig. 4b–d) are consistent with ultrathin TiO_2 coating of the MWCNTs. It is well-known that the mass ratio tetrabutyl titanate : MWCNTs plays an important role in the mass loading of TiO_2 and the morphology of the resultant nanocomposites.[32] From Fig. 4b–d, it can be seen that the MWCNTs in the nanocomposites are decorated with many small TiO_2 nanoparticles, resulting in the coarse surface of the MWCNTs. The corresponding HRTEM image (Fig. S4†) shows that the TiO_2 nanoparticles are strongly coupled to the MWCNTs, which may be due to the interactions between the hydroxyl groups of the hydrolyzed TiO_2 precursors and the oxygen-containing groups (such as –COOH) on the MWCNTs.[33] The mass loading of TiO_2 on the MWCNTs and the diameter of the coated MWCNTs increase with increasing mass ratio of tetrabutyl titanate : MWCNTs (M0.25 < M0.50 < M1.00), which is consistent with the Raman results. No free TiO_2 nanoparticles (detached from the MWCNTs) can be seen in the TEM images. Although information obtained from TEM should not be over-interpreted, this method still provides complementary evidence for successful preparation of TiO_2 decorated MWCNTs.

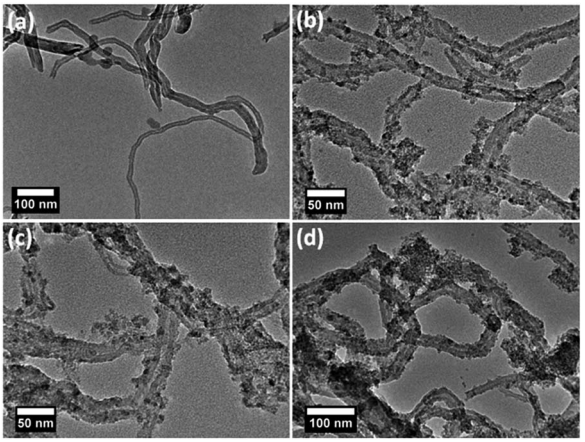

Fig. 4 TEM spectra of the MWCNTs (a) and the M0.25 (b), M0.50 (c) and M1.00 (d) nanocomposites.

Table 1 Integrated intensity ratio of the E_g anatase peak (I_A) and the disordered carbon peak (I_D) of the Raman spectra

Sample	M0.25	M0.50	M1.00
I_A/I_D	14.0	31.25	178.57

Photophysical properties

The influence of the MWCNTs on the diffuse reflectance UV/vis spectra is apparent from considering the optical absorption spectra of all samples (Fig. 5); for comparison, the TiO_2 nanoparticles were also measured under the same conditions. As expected, pure TiO_2 shows a characteristic absorption edge at 400 nm (Fig. 5a), which is ascribed to charge transfer from the valence band (mainly formed by 2p orbitals of the oxide anions) to the conduction band (mainly formed by 3d t_{2g} orbitals of the Ti^{4+} cations).[34] The presence of different amounts of TiO_2 significantly affects the optical absorption of the TiO_2/MWCNT nanocomposites. Compared to TiO_2, all of the TiO_2/MWCNT nanocomposites show a higher absorbance. In addition, for

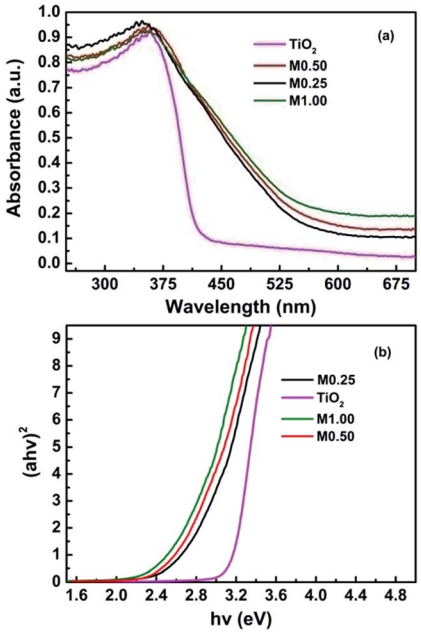

Fig. 5 (a) UV-vis diffuse reflectance spectra of the TiO_2, M0.25, M0.50 and M1.00 samples; (b) plot of the transformed Kubelka–Munk function *versus* the energy of light.

M0.25, M0.50 and M1.00, the absorption edge is red shifted to longer wavelengths, which is probably due to the creation of oxygen vacancies during the growth of TiO_2 on the MWCNTs.[35] The TiO_2/MWCNTs nanocomposites all show unusual UV/vis spectra, with broad absorptions through the entire UV/vis region, consistent with the interaction of TiO_2 and MWCNT in the nanocomposites narrowing the band gap of TiO_2. A plot of the transformed Kubelka–Munk function as a function of energy of light is shown in Fig. 5b, from which the estimated band gaps are 3.16, 2.58, 2.49 and 2.43 eV corresponding to bare TiO_2, M0.25, M0.50 and M1.00, respectively. This supports the qualitative observation of a red shift in the absorption edge of the TiO_2/MWCNT nanocomposites as compared to the bare TiO_2, analogous to observations with carbon-doped TiO_2 nanoparticles.[36] The TiO_2/MWCNT composites can therefore be excited more easily than TiO_2 to produce electron–hole pairs, improving the charge transfer from the valence band to the conduction band.

TiO_2 has a direct band gap but with dipole–forbidden transitions, so it is difficult to observe photoluminescence with bulk TiO_2.[37] However, photoluminescence signals can be observed for TiO_2 nanoparticles. Fig. 6 shows photoluminescence spectra of pure TiO_2 and the TiO_2/MWCNT nanocomposites (M0.25, M0.50 and M1.00) excited at a wavelength of 300 nm. As can be seen from this figure, similar photoluminescence spectra were observed for all samples. The growth of TiO_2 on MWCNTs yields oxide particles with a very high density of oxygen vacancies. These vacancies give rise to in-gap states or surface states that yield a continuum of below bandgap absorbances. Such defects are the likely origin of the observed photoluminescence at 392 nm and in the wavelength range from 450 to 500 nm.[37] However,

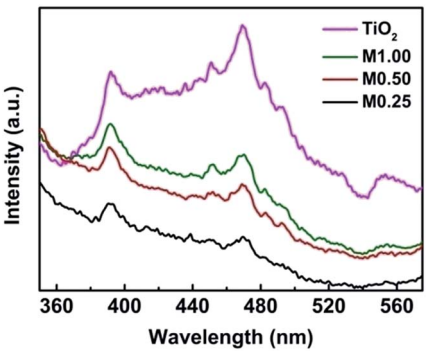

Fig. 6 Photoluminescence spectra of the TiO_2, M0.25, M0.50 and M1.00 samples.

it should be noted that although the presence of defects can be easily and efficiently proved by photoluminescence measurements, assignment of the different bands is still an area of intense debate within the literatures, because the photoluminescence can result from defects on the surface of TiO_2,[38,39] the oxygen vacancies,[40,41] the self-trapped excitons,[38,39] or from the charge carrier trapping, migration, and transfer.[42,43] Variation of photoluminescence intensity may originate from the change of defect state on the shallow level of the TiO_2 surface.[41] The peak intensities in the photoluminescence spectra of the TiO_2/MWCNT nanocomposites are lower than that of pure TiO_2, and increase as the TiO_2 loading increases. If the photoluminescence emission mainly results from the recombination of excited electrons and holes, the low photoluminescence intensity indicates a decrease in recombination efficiency.[44] Since MWCNTs have a large number of one-dimensional concentric graphitic tubes, which can transfer electrons with no electrical resistance, TiO_2/MWCNTs can also transfer photoelectrons generated from TiO_2 under light excitation easily.[45]

Nonlinear optical properties

Optical limiters are materials that exhibit high transmittance for low level inputs while blocking the transmittance of high-intensity laser beams.[46,47] Such materials have potential for the protection of optical sensors from possible damage caused by intense laser pulses, and also have potential in optical switching and other areas.[48] The open-aperture Z-scan method was used to investigate the third-order nonlinear optical properties in both the picosecond (ps) and nanosecond (ns) regimes. The ps Z-scan studies were performed at an excitation wavelength of 532 nm with a 21 ps pulse width, while the ns measurements were carried out at 532 nm with a pulse width of 4 ns. For ease of comparison, dispersions of all samples were adjusted to have the same linear transmittance (60% at 532 nm) by varying their concentration. In open-aperture Z-scan measurements, the transmittance of the sample is measured as the sample is translated through the focal point. As the sample is translated towards the focal point, the laser pulse intensity increases and the nonlinear response becomes measurable, resulting in a decreasing or an increasing transmittance due to different nonlinear mechanisms. Experiments

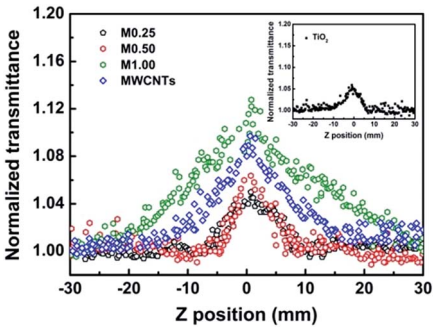

Fig. 7 Open-aperture Z-scan curves for MWCNTs, M0.25, M0.50 and M1.00 at 532 nm in the ps regime. Shown in the inset is the open-aperture data of TiO_2.

with DMF solvent displayed no obvious NLO response under the same experimental conditions, indicating that the solvent contribution is negligible; the observed NLO response should thus be assigned solely to the solutes.

Fig. 7 contains the open-aperture Z-scan traces of TiO_2, MWCNTs, M0.25, M0.50 and M1.00 dispersions using ps laser pulses. The normalized transmittance of all samples increase as the sample is brought closer to the focal point, suggesting saturable absorption.[49] Thus, these samples can effectively suppress low intensity light but allow higher intensity light to pass.[50] In these Z-scan traces, the saturable absorption signal increases in the order: M0.25 < TiO_2 < M0.50 < MWCNTs < M1.00, the results indicating that the saturable absorption of MWCNTs can be tuned by varying the TiO_2 content. The nanocomposite M1.00 is therefore a better candidate than the pristine MWCNTs for saturable absorber applications such as pulse shaping or as shutters in ps systems.

With 4 ns pulses, all Z-scan traces (except those of TiO_2 dispersions) show a decrease in transmittance at the focal point (Fig. 8), typical of an induced positive nonlinear absorption of incident light, indicating clear optical limiting. At the focal point, the transmittance of the M0.25, M0.50, MWCNTs and M1.00 dispersions drops to 83%, 79%, 68% and 59%, respectively. The depth of the valley in the open-aperture Z-scan suggests the extent of the nonlinear behavior. In contrast to M1.00 dispersions, a relatively weak NLO effect was noted with samples M0.25 and M0.50, inferior to that of the MWCNTs. For a quantitative comparison, we have performed a theoretical fitting of the experimental results to obtain effective nonlinear absorption coefficients β_{eff} (m W^{-1}). With the same linear transmittance (60% at 532 nm), M1.00 displays a better nonlinear absorption response [β_{eff} 4.2×10^{-10} m W^{-1} *c.f.* those of M0.25 (1.2×10^{-10} m W^{-1}), M0.50 (1.5×10^{-10} m W^{-1}) and MWCNTs (2.7×10^{-10} m W^{-1})], implying a significant influence of the TiO_2 content in these nanocomposites on the nonlinear absorption performance and further verifying the advantage of M1.00 as a nonlinear material. Similar phenomena have been observed with organically modified silicate–MWCNT nanohybrid gel glass (MWCNT–Ormosil).[51] M1.00 has a larger β_{eff} value than the MWCNT–Ormosil system in ref. [51], although the differing experimental geometries render such a comparison necessarily cautious.

The OL performance of these materials was also assessed using 4 ns pulsed laser irradiation at 532 nm (Fig. 9). At low input fluence, dispersions of these species (MWCNTs, M0.25, M0.50 and M1.00) exhibit linear output fluences, obeying Beer's Law. However, as the incident fluence increases, the output fluence deviates from linearity, consistent with an OL effect. At the same linear transmittance, M1.00 dispersions possess a relatively better OL response than the other three materials, consistent with the results from nonlinear absorption studies. For example, at a fluence of 1.2 J cm^{-2}, the output fluence from M1.00 dispersions is 0.1 J cm^{-2}, significantly less than the output of the other samples from the present studies, and consistent with the TiO_2 content of the nanocomposites influencing the OL behavior. The optical nonlinearity of pure TiO_2 (Fig. 8 and 9) was also investigated under the same experimental conditions, but no obvious signal was observed, suggesting that TiO_2 has a very small NLO effect that can be neglected in the present case.

As mentioned above, a concentration-dependent NLO response was observed for the TiO_2/MWCNT nanocomposites. The OL behavior of the MWCNTs is dominated by nonlinear scattering, the same mechanism as that exhibited by carbon black suspension.[52] In the scattering process, heating from the laser pulses leads to vaporization and ionization of the MWCNTs, and the resultant rapid formation of micrometer-

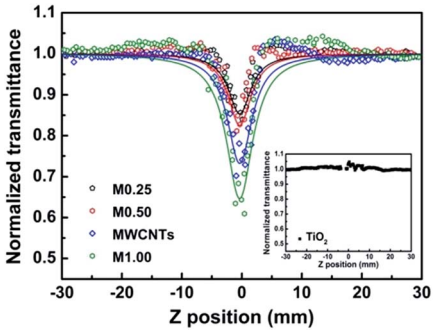

Fig. 8 Plot of normalized transmittance against *z* position for the MWCNTs and the M0.25, M0.50 and M1.00 nanocomposites at 532 nm in the ns regime. Shown in the inset is the open-aperture data of TiO_2. Solid curves represent the theoretical fits to the experimental data.

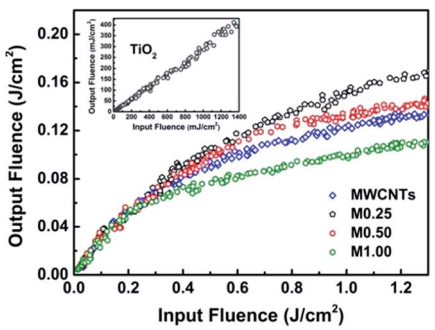

Fig. 9 Optical limiting curves for the MWCNTs and the M0.25, M0.50 and M1.00 nanocomposites at 532 nm in the ns regime. Shown in the inset is the optical limiting response of TiO_2.

sized plasmas.[53] These microplasmas can act as scattering centers and strongly scatter light from the transmitted beam direction, resulting in an increase in limiting response. Thus, nonlinear scattering, arising from MWCNT moieties, is proposed as one of the main mechanisms for enhanced OL response seen with this nanocomposite. Significant fluorescence quenching of TiO_2 following doping with MWCNTs is observed, which may inhibit recombination of the electron–hole pairs, and therefore accelerate the transfer of photogenerated electrons. During the preparation of the M1.00 nanocomposite, some oxygen-containing groups on the surface of the MWCNTs are partially removed by hydro-thermal treatment, the conjugation thereby being extended. The more extended the conjugation, the greater the chance for electron/energy transfer, leading to enhanced OL performance. The increased OL in M1.00 may also have a significant contribution from defect-induced states generated during preparation. The presence of defects can be confirmed by the increased I_D/I_G ratio (Fig. 3) after hydro-thermal treatment, implying an increase in the number of defects in the sample M1.00.[54] The detailed mechanism needs further investigation, but the current work demonstrates that the OL performance of the M1.00 TiO_2/MWCNT nanocomposite is a sensitive function of a combination of the NLO mechanisms operative with MWCNTs and TiO_2.

Conclusions

A hydrothermal route to TiO_2/MWCNT nanocomposites (M0.25, M0.50 and M1.00) has been demonstrated. The formation of nanocomposites was confirmed by FTIR, Raman and XPS spectroscopies, XRD, and TEM. The viability of MWCNT/TiO_2 nanocomposites as nonlinear optical materials has been examined using the Z-scan technique at 532 nm with both 4 ns and 21 ps laser pulses, and the NLO and optical limiting performance have been found to depend on the TiO_2 content. The results show that M1.00 displays a better nonlinear absorption response than the other three materials. The best optical limiting response in the nanosecond regime was also observed for the M1.00 nanocomposite, and this is suggested to result from a combination of mechanisms. This nanohybrid is a promising candidate for optical limiting and solar-energy conversion applications.

Experimental

Materials

MWCNTs with average diameters of 20-30 nm and lengths of 10-30 μm were obtained from Beijing DK Nanotechnology Co., China, and used as received. The purity of the MWCNTs was 95%. Tetrabutyl titanate and anhydrous ethanol were supplied by Shanghai Sinopharm Chemical Reagent Co. All other reagents were purchased from a commercial supplier and used without further purification, unless otherwise stated. Distilled water was used for all experiments.

Instruments and measurements

Fourier-transform infrared (FTIR) spectra were recorded with a MB154S-FTIR spectrometer (Canada) in pellets of spectroscopic grade KBr. Ultraviolet-visible (UV-vis) diffuse reflectance spectra were recorded using a Varian Cary 500 spectrophotometer equipped with a diffuse reflectance accessory at room temperature in the range 200-800 nm. A $BaSO_4$ pellet was used as a reflectance standard. Fluorescence spectra were measured using a Fluoro-Max-P spectrofluorimeter. Raman spectra were recorded at room temperature on a Renishaw inVia Raman Microscope, exciting at 532 nm with Ar^+ radiation. The laser light was focused onto samples by using a microscope equipped with an a × 100 objective. XRD patterns of all samples were recorded on a XD-3 diffractometer with Cu Kα radiation (λ = 0.15418 nm) (Beijing Purkinje General Instrument Co., China). Transmission electron microscopy (TEM) and high-resolution transmission electron microscopy (HRTEM) experiments were performed with a JEM-2100 (JEOL), working at 200 kV. Samples for TEM and HRTEM analysis were obtained by spreading a drop of a dilute dispersion of the as-prepared products on amorphous carbon-coated copper grids that were then dried in air before transfer to the TEM or HRTEM sample chamber. X-ray photoelectron spectroscopy (XPS) characterization was performed on a RBD upgraded PHI-5000C ESCA (PerkinElmer) electron spectrometer with a Mg Kα line at 280 eV.

Z-scan measurements were carried out employing a Q-switched Nd:YAG laser with linearly polarized 4 ns and 21 ps pulses at 532 nm.[55] To avoid thermal accumulation in the sample, a low repetition rate of 2 Hz was used, ensuring that each pulse of light encountered fresh sample. The laser beam was focused by a 30 cm focusing lens, after spatially removing higher-order modes. To facilitate comparison, all sample concentrations were adjusted to 0.15 mg mL^{-1}; all samples were examined in a 2 mm thick quartz cell and adjusted to have the same transmittance. Two pyroelectric energy probes were used to monitor the input fluence and the fluence of the transmitted beam at regular intervals, as the sample was translated along the propagation direction of the focused Gaussian beam.

Preparation of TiO_2-decorated MWCNT nanocomposites

TiO_2/MWCNT nanocomposites were prepared by using a hydrothermal method. In a typical synthesis, MWCNTs (50 mg) were first sonicated in a mixture of deionized H_2O (6 mL) and EtOH (3 mL). Tetrabutyl titanate was then added to the MWCNT dispersion, followed by sonication for 30 min to obtain a homogeneous suspension. The suspension was then placed in a 10 mL Teflon-sealed autoclave and maintained at 160 °C for 72 h. The resultant materials were collected by centrifugation, washed thoroughly with deionized water several times, rinsed with EtOH, and then dried under vacuum at room temperature for 24 h to produce a grayish powder of TiO_2/MWCNT nanocomposites. To investigate the effect of TiO_2 content on the NLO properties of the TiO_2/MWCNT composites, composites with different loadings of TiO_2 were prepared by changing the mass ratio of tetrabutyl titanate (the precursor of TiO_2)/MWCNTs from 5 : 1 to 10 : 1 and 20 : 1, the resultant samples being

referred to as M*x*, where *x* relates to the mass in grams of tetrabutyl titanate (0.25, 0.50, or 1.00). For comparison, pure TiO_2 was also prepared *via* a hydrothermal route under the same conditions but without the addition of the MWCNTs.

Acknowledgements

Financial support from the National Natural Science Foundation of China (51432006, 50925207, 51172100), the Ministry of Science and Technology of China for the International Science Linkages Program (2011DFG52970), the Ministry of Education of China for the Changjiang Innovation Research Team (IRT13R24), the Ministry of Education and the State Administration of Foreign Experts Affairs for the 111 Project (B13025), 100 Talents Program of CAS, Jiangsu Innovation Research Team and Jiangsu Province (2013-479) are gratefully acknowledged. M. G. H. and C. Z. thank the Australian Research Council (ARC) for support.

Notes and references

1 N. Karousis, N. Tagmatarchis and D. Tasis, *Chem. Rev.*, 2010, **110**, 5366.
2 D. M. Guldi, G. M. A. Rahman, N. Jux, D. Balhino, N. Tagmatachis and M. Prato, *Chem. Commun.*, 2005, 2038.
3 C. Ehli, D. M. Guldi, M. Á. Herranz, N. Martín, S. Campidelli and M. Prato, *J. Mater. Chem.*, 2008, **18**, 1498.
4 R. H. Baughman, A. A. Zakhidov and W. A. de Heer, *Science*, 2002, **297**, 787.
5 V. Georgakilas, K. Kordatos, M. Prato, D. M. Guldi, M. Holzinger and A. Hirsch, *J. Am. Chem. Soc.*, 2002, **124**, 760.
6 Y. P. Sun, K. Fu, Y. Lin and W. J. Huang, *Acc. Chem. Res.*, 2002, **35**, 1096.
7 X. Sun, R. Q. Yu, G. Q. Xu, T. S. A. Hor and W. Ji, *Appl. Phys. Lett.*, 1998, **73**, 3632.
8 A. J. Wang, L. L. Long, W. Zhao, Y. L. Song, M. G. Humphrey, M. P. Cifuentes, X. Z. Wu, Y. S. Fu, D. D. Zhang, X. F. Li and C. Zhang, *Carbon*, 2013, **53**, 327.
9 O. Muller, Y. Lutz, A. Tessier, J. P. Moeglin and V. Keller, *Appl. Opt.*, 2010, **49**, 1097.
10 K. Balasubramanian and M. Burghard, *Small*, 2005, **1**, 180–192.
11 H. J. Lee, S. J. Oh, J. Y. Choi, J. W. Kim, J. Han and J. B. Baek, *Chem. Mater.*, 2005, **17**, 5057.
12 M. Xu, T. Zhang, B. Gu, J. Wu and Q. Chen, *Macromolecules*, 2006, **39**, 3540.
13 N. He, Y. Chen, J. R. Bai, J. Wang, W. J. Blau and J. H. Zhu, *J. Phys. Chem. C*, 2009, **113**, 13029.
14 Z. B. Liu, Z. Guo, X. L. Zhang, J. Y. Zheng and J. G. Tian, *Carbon*, 2013, **51**, 419.
15 J. S. Lee, K. H. You and C. B. Park, *Adv. Mater.*, 2012, **24**, 1084.
16 M. R. Hoffmann, S. T. Martin, W. Choi and D. W. Bahnemann, *Chem. Rev.*, 1995, **95**, 69.
17 K. Woan, G. Pyrgiotakis and W. Sigmund, *Adv. Mater.*, 2009, **21**, 2233.
18 S. Muduli, W. Lee, V. Dhas, S. Mujawar, M. Dubey, K. Vijayamohanan, S. H. Han and S. Ogale, *ACS Appl. Mater. Interfaces*, 2009, **4**, 2030.
19 A. H. Yuwono, J. Xue, J. Wang, H. I. Elim, W. Ji, Y. Li and T. J. White, *J. Mater. Chem.*, 2003, **13**, 1475.
20 A. H. Yuwono, B. Liu, J. Xue, J. Wang, H. I. Elim, W. Ji, Y. Li and T. J. White, *J. Mater. Chem.*, 2004, **14**, 2978.
21 M. Hari, S. A. Joseph, S. Mathew, P. Radhakrishnan and V. P. N. Nampoori, *J. Appl. Phys.*, 2012, **112**, 074307.
22 K. M. Rahulan, L. D. Stephen and C. C. Kanakam, *Appl. Surf. Sci.*, 2013, **266**, 326.
23 K. Lliopoulos, G. Kalogerakis, D. Vernardou, N. Katsarakis, E. Koudoumas and S. Couris, *Thin Solid Films*, 2009, **518**, 1174.
24 M. K. Kavitha, H. John, P. Gopinath and R. Philip, *J. Mater. Chem. C*, 2013, **1**, 3669.
25 K. M. Rahulan, S. Ganesan and P. Aruna, *Adv. Nat. Sci.: Nanosci. Nanotechnol.*, 2011, **2**, 025012.
26 H. Wang, H. L. Wang, W. F. Jiang and Z. Q. Li, *Water Res.*, 2009, **43**, 204.
27 C. Song, P. Chen, C. Y. Wang and L. Y. Zhu, *Chemosphere*, 2012, **86**, 853.
28 N. G. Akalework, C. J. Pan, W. N. Su, J. Rick, M. C. Tsai, J. F. Lee, J. M. Lin, L. D. Tsai and B. J. Hwang, *J. Mater. Chem.*, 2012, **22**, 20977.
29 A. M. Tonejc, I. Djerdj and A. Tonejc, *Mater. Sci. Eng., C*, 2002, **19**, 85.
30 K. R. Zhu, M. S. Zhang, Q. Chen and Z. Yin, *Phys. Rev. Lett.*, 2005, **340**, 224.
31 X. B. Yan, B. K. Tay and Y. Yang, *J. Phys. Chem. B*, 2006, **110**, 25844.
32 W. Jarenboon, S. Pimanpang, S. Maensiri, E. Swatsitang and V. Amornkitbamrung, *J. Alloys Compd.*, 2009, **476**, 840.
33 Q. J. Xiang, J. G. Yu and M. Jaroniec, *Nanoscale*, 2011, **3**, 3670.
34 S. Sakthivel, M. V. Shankar, M. Palanichamy, B. Arabindoo, D. W. Bahnemann and V. Murugesan, *Water Res.*, 2004, **38**, 3001.
35 D. C. Cronemeyer, *Phys. Rev.*, 1959, **113**, 1222.
36 S. Sakthivel and H. Kisch, *Angew. Chem., Int. Ed.*, 2003, **42**, 4908.
37 C. Y. Yen, Y. F. Lin, S. H. Liao, C. C. Weng, C. C. Huang, Y. H. Hsiao, C. C. M. Ma, M. C. Chang, H. Shao, M. C. Tsai, C. K. Hsieh, C. H. Tsai and F. B. Weng, *Nanotechnology*, 2008, **19**, 375305.
38 B. Choudhury, M. Dey and A. Choudhury, *Appl. Nanosci.*, 2014, **4**, 499.
39 E. S. Junior, F. A. L. Porta, M. S. Liu, J. Andrés, J. A. Varela and E. Longo, *Dalton Trans.*, 2015, **44**, 3159.
40 N. O. Ramoraswi and P. G. Ndungu, *Nanoscale Res. Lett.*, 2015, **10**, 427.
41 A. Ali, I. Ruzybayev, E. Yassitepe, S. I. Shah and A. S. Bhatti, *J. Phys. Chem. C*, 2013, **117**, 19517.
42 J. G. Yu, H. G. Yu, B. Cheng, X. J. Zhao, J. C. Yu and W. K. Ho, *J. Phys. Chem. B*, 2003, **107**, 13871.
43 D. H. Kim, D. K. Choi, S. J. Kim and K. S. Lee, *Catal. Commun.*, 2008, **9**, 654.
44 F. B. Li and X. Z. Li, *Appl. Catal., A*, 2002, **228**, 15.

45 J. W. Liu, J. Li, A. Sedhain, J. Y. Lin and H. X. Jiang, *J. Phys. Chem. C*, 2008, **112**, 17127.
46 Z. Guo, F. Du, D. M. Ren, Y. S. Chen, J. Y. Zheng, Z. B. Liu and J. Q. Tian, *J. Mater. Chem.*, 2006, **16**, 3021.
47 C. F. Li, L. Zhang, M. Yang, H. Wang and Y. X. Wang, *Phys. Rev. A*, 1994, **49**, 1149.
48 G. Argouarch, R. Veillard, T. Roisnel, A. Amar, H. Meghezzi, A. Boucekkine, V. Hugues, O. Mongin, M. Blanchard-Desce and F. Paul, *Chem.–Eur. J.*, 2012, **18**, 11811.
49 M. Yüksek, U. Kürüm, H. G. Yaglioglu, A. Elmali and A. Ateş, *J. Appl. Phys.*, 2010, **107**, 033115.
50 K. P. Wang, J. Wang, J. T. Fan, M. Lotya, A. O'Neill, D. Fox, Y. Y. Feng, X. Y. Zhang, B. X. Jiang, Q. Z. Zhao, H. Z. Zhang, J. N. Coleman, L. Zhang and W. J. Blau, *ACS Nano*, 2013, **7**, 9260.
51 C. Zheng, M. Feng, Y. H. Du and H. B. Zhan, *Carbon*, 2009, **47**, 2889.
52 B. Anand, S. A. Ntim, V. S. Muthukumar, S. S. S. Sai, R. Philip and S. Mitra, *Carbon*, 2011, **49**, 4767.
53 D. M. Guldi, H. Taieb, G. M. A. Rahman, N. Tagmatarchis and M. Prato, *Adv. Mater.*, 2005, **17**, 871.
54 V. A. Coleman, R. Knut, O. Karis, H. Grennberg, U. Jansson, R. Quinlan, B. C. Holloway, B. Sanyal and O. Eriksson, *J. Phys. D: Appl. Phys.*, 2008, **41**, 062001.
55 A. J. Wang, L. L. Long, S. C. Meng, X. F. Li, W. Zhao, Y. L. Song, M. P. Cifuentes, M. G. Humphrey and C. Zhang, *Org. Biomol. Chem.*, 2013, **11**, 4250.